ACS Catalysis

Research Article

Cite This: ACS Catal. 2019, 9, 902−911

pubs.acs.org/acscatalysis

Adsorption and Destruction of the G-Series Nerve Agent Simulant Dimethyl Methylphosphonate on Zinc Oxide

Scott Holdren,[†,⊥] Roman Tsyshevsky,[‡,⊥] Kenan Fears,[∥] Jeffrey Owrutsky,[∥] Tao Wu,[†] Xizheng Wang,[†] Bryan W. Eichhorn,[†] Maija M. Kuklja,*[,‡] and Michael R. Zachariah*[,†,§]

[†]Department of Chemistry and Biochemistry, University of Maryland, College Park, Maryland 20742, United States

[‡]Materials Science and Engineering Department, University of Maryland, College Park, Maryland 20742, United States

[§]Department of Chemical and Biomolecular Engineering, University of Maryland, College Park, Maryland 20742, United States

[∥]Chemistry Division, U.S. Naval Research Laboratory, Washington, DC 20375, United States

Supporting Information

ABSTRACT: Organophosphorus chemical warfare agents (CWAs) are extremely toxic compounds that are nominally mitigated with gas mask filtration employing metal oxide impregnated activated carbon filtration material. To develop more effective sorbents, it is important to understand the surface chemistry between these organophosphorus compounds and the individual components that make up these filtration materials. In this study, density functional theory (DFT) and Fourier transform infrared spectroscopy (FTIR) were employed to investigate the adsorption and decomposition mechanisms between a sarin simulant molecule, dimethyl methylphosphonate (DMMP), and zinc oxide, which is a component found in current filtration materials. Theoretical calculations show that DMMP readily adsorbs to a pristine and hydroxylated ZnO $(10\bar{1}0)$ surface with average adsorption energies of 132 and 65 kJ mol^{-1}, respectively. Experimental diffuse reflectance fourier transform infrared spectroscopy (DRIFTS) reveals that ZnO adsorbs water and readily hydroxylates under ambient conditions, which can facilitate adsorption through hydrogen bonding of the P═O to ZnO surface hydroxyls. FTIR gas phase analysis also reveals that DMMP decomposes in the presence of ZnO nanoparticles (NPs) to produce methanol at room temperature. Assuming a fully hydroxylated surface of ZnO, DFT calculations reveal several plausible mechanisms for DMMP decomposition to form methanol with an activation energy barrier of 99.6 kJ mol^{-1}. On the basis of this energy barrier to decompose DMMP, a turnover frequency (TOF) of only 3.5×10^{-7} s^{-1} is calculated assuming full coverage of DMMP on the ZnO nanoparticles tested. This value is qualitatively consistent with experimental results.

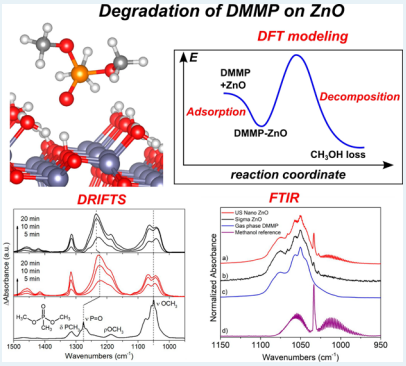

KEYWORDS: *ZnO, chemical warfare agent, DFT, DRIFTS, hydroxyl, decontamination, filtration*

1. INTRODUCTION

Discovery and design of new filter materials for advanced filter technologies requires a fundamental understanding of how these materials interact with pollutants and toxins. A primary barrier impeding both advancement of our knowledge and the search for improved filter materials for adsorption and destruction of chemical warfare agents (CWA) is their high toxicity. Experiments involving these compounds are usually carried out in specially equipped facilities. To fill the gaps in the understanding of CWA interactions with existing and potential filter materials, actual toxins in many laboratory experiments are replaced with less hazardous simulant compounds.

We employed this approach by studying the surface interactions of an organophosphorus CWA simulant dimethyl methylphosphonate (DMMP, Figures 1 and 2a) with zinc oxide, which is one of the components of the ASZM-TEDA carbon-based filter material used in gas masks.[1] DMMP is a CWA simulant commonly employed to study the adsorption interactions of G-series nerve agents such as sarin, which is a notorious toxic CWA frequently used in chemical attacks. DMMP has certain structural similarities to the G-series nerve agents shown in Figure 1. Most notably, all of the structures contain the P═O bond, which is the primary mode used to bind to metal oxides.

Here, we report results of our theoretical and experimental study of DMMP adsorption and decomposition on ZnO surfaces. Despite many experimental attempts to study the interaction of DMMP with metal oxides,[2−17] very little is known about mechanisms that govern decomposition of DMMP and the role of surface morphology and electronic properties on these processes.[18,19] It is commonly accepted that DMMP initially interacts with an oxide surface through its phosphoryl oxygen and forms a bond with one of the Lewis acid sites on the surface (e.g., an under-coordinated metal atom),[2,5,7,9,20] whereas breaking of a P−OCH_3 bond through

Received: July 29, 2018
Revised: December 12, 2018
Published: December 14, 2018

DOI: 10.1021/acscatal.8b02999
ACS Catal. 2019, 9, 902−911

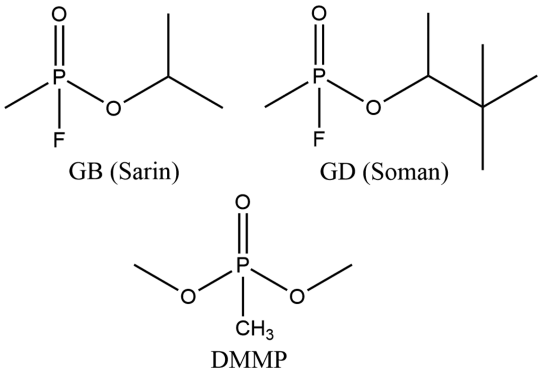

Figure 1. Chemical warfare nerve agents sarin (left), soman (right), and CWA simulant DMMP (bottom).

an electrophilic or nucleophilic attack involving surface hydroxyls is usually invoked as the main decomposition mechanism of DMMP.[18,19] Methanol, dimethyl ether, and surface methoxy groups are among the main products of DMMP decomposition on oxide surfaces at room temperature. It has also been shown that DMMP decomposition on metal oxides at elevated temperatures leads to additional products including formaldehyde, methane, carbon dioxide, carbon monoxide, and hydrogen.[4,6,10,11,21] The role of surface hydroxyls in DMMP adsorption and decomposition on MoO_3,[12] $(MoO_3)_3$ clusters,[13] zirconium hydroxide,[14,22] and zirconium-based metal organic frameworks[15] has been recently studied using various experimental techniques and DFT modeling. We have also explored the interaction and reaction products of DMMP with metal oxide surfaces including MoO_2[16] and CuO[17] by ambient pressure X-ray photoelectron spectroscopy (APXPS), diffuse reflectance infrared Fourier transform spectroscopy (DRIFTS), and DFT modeling. These studies show that reaction pathways are, not surprisingly, dependent on oxide type, and thus CuO facilitates cleavage of $PO-CH_3$, $P-OCH_3$ and $P-CH_3$ bonds, while MoO_2 proceeds mainly through breaking of $PO-CH_3$ and $P-OCH_3$ bonds.

ZnO surface chemistry has been of significant interest because of its uses in catalytic processes such as the water gas shift reaction[23−26] and as a toxic gas sensor material.[27−30] In particular, Yoo et al. has investigated the sensing properties of Al-doped ZnO nanoparticles toward DMMP and finds that Al doped ZnO exhibits high sensitivity (~100 ppb) mainly due to the oxygen vacancies created by the Al^{3+} dopant.[30] In addition, ZnO based materials have also shown high selectivity toward DMMP relative to other gases such as NH_3, CO, and organic compounds (e.g., acetone and ethanol).[28,30] Zinc oxide has also generated interest as a sorbent/decontaminant material to a variety of CWAs including sarin[31] and mustard gas.[32] Other studies also revealed high activity of ZnO nanoparticles toward adsorption and decomposition of mustard agent simulants, in solutions such as isopropanol, acetone, and *n*-hexane.[33,34] Nevertheless, there are numerous open questions regarding mechanisms of DMMP adsorption and decomposition on ZnO.

In this work, DFT modeling was used to explore mechanisms, energetics, and product vibrational frequencies for DMMP adsorption and degradation on pristine and hydroxylated ZnO $(10\bar{1}0)$ surfaces. DRIFTS of adsorbed species and FTIR headspace product measurements were performed on ZnO nanoparticles to compare with the computational results.

2. METHODS

2.1. DFT Modeling. Solid state periodic calculations were performed by density functional theory (DFT) with PBE[35] and projector augmented-wave (PAW)[36] pseudopotentials as implemented in the VASP code.[37−39] In simulating an ideal ZnO wurzite crystal (Figure 2b), we used a 6 × 6 × 6 Monkhorst−Pack k-point mesh with a kinetic energy cutoff of 520 eV. Atomic coordinates and lattice constants were allowed to simultaneously relax without any symmetry constraints. The convergence criterion for electronic steps was set to 10^{-5} eV, and the maximum force acting on any atom was set not to exceed 0.02 eV $Å^{-1}$. The calculated lattice parameters of the ZnO hexagonal unit cell (Figure 2b), $a = b = 3.27$ Å and $c = 5.25$ Å, agree with the experimental lattice vectors[40] within ~1%.

In modeling adsorption and decomposition reactions on ZnO, we chose the thermodynamically favorable $(10\bar{1}0)$ surface.[41] In the ZnO surface calculations (Figure 2c), a surface slab was cut from the bulk ZnO structure to form the $(10\bar{1}0)$ surface with the supercell containing 240 atoms and lattice parameters of $a = 16.35$ Å, $b = 15.76$ Å, and $c = 29.44$ Å. A vacuum layer of 20 Å was placed on top of the ZnO $(10\bar{1}0)$

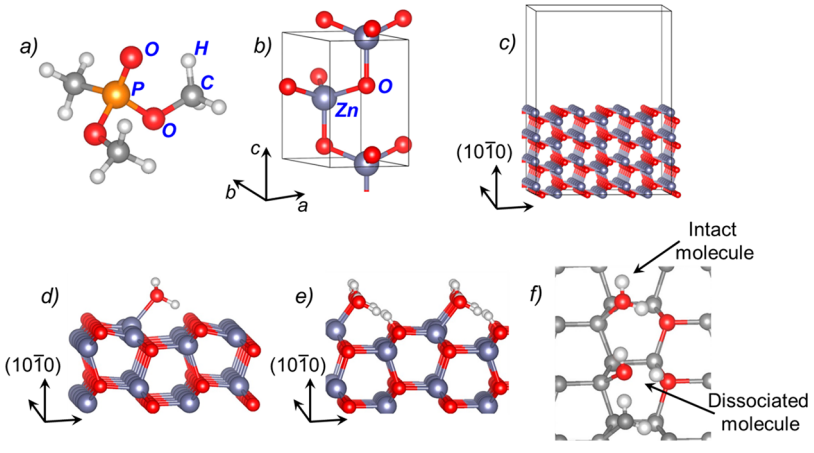

Figure 2. Structures of (a) DMMP, (b) the ZnO unit cell, (c) the ZnO $(10\bar{1}0)$ surface supercell model (denoted "pristine" surface), (d) the ZnO $(10\bar{1}0)$ surface with adsorbed water molecule; (e) side and (f) top views of water monolayers on the ZnO $(10\bar{1}0)$ surface.

DOI: 10.1021/acscatal.8b02999
ACS Catal. 2019, 9, 902−911

surface to minimize interactions between the supercells in the z-direction and to avoid any significant overlap between wave functions of periodically translated cells. A PBE+D2[35,42,43] functional, which includes corrections for weak van der Waals interactions, was used to calculate adsorption energies. Minimal energy paths in the VASP periodic calculations were obtained with the nudged elastic band method[44] with five intermediate images. Atomic positions were relaxed using conjugate gradient and quasi-Newtonian methods within a force tolerance of 0.05 Å eV^{-1}. Vibrational frequencies were calculated using the finite difference approach.

To study the effect of water on the adsorption and decomposition of DMMP, we employed two models. In the first model (Figure 2d), the supercell contains one water molecule adsorbed on the ZnO $(10\bar{1}0)$ surface. In the second model (Figures 2e and f), the ZnO $(10\bar{1}0)$ surface is covered with a monolayer of water containing intact and dissociated water molecules (see refs 41, 45). Our calculations showed that a single water molecule per supercell (corresponding to only 0.016 water molecules per one surface ZnO moiety), unlike a monolayer of water, does not have any strong effect on the activation energy of DMMP destruction on the ZnO surface. However, the presence of a water molecule opens new decomposition pathways associated with methanol elimination from DMMP. Therefore, we will only consider results obtained using a model with a monolayer of water on ZnO in this work. The results obtained for the model with a single water molecule per supercell and its corresponding discussion can be found in the Supporting Information.

2.2. Experimental Section. *2.2.1. Materials.* ZnO nanopowder (99+%, 35−45 nm) from US Research Nanomaterials (abbreviation US Nano) and ZnO nanopowder (<100 nm particle size) from Sigma-Aldrich (abbreviation Sigma) were used for these analyses. Dimethyl methylphosphonate (DMMP 97%) was purchased from Sigma-Aldrich and was used as received.

2.2.2. Characterization of ZnO Nanoparticles. X-ray diffraction (XRD) was performed with a Bruker D8 diffractometer with Cu Kα radiation. XRD patterns of both ZnO nanoparticles (NPs) identified that they are hexagonal with a wurtzite structure. A Le Bail refinement determined the lattice constants for both ZnO NPs using literature ZnO hexagonal wurtzite as a reference (JCPDF 01-089-7102).[46] The XRD patterns and lattice constants determined from the refinement can be found in the Supporting Information (Figure S1). The experimentally determined lattice constants were in excellent agreement (within 1%) of our DFT calculated lattice parameters (refer to SI).

Thermogravimetric analysis coupled with mass spectrometry (TGA-MS) measurements were made using a TA Instruments SDT-Q600 and Discovery Mass spectrometer. For each run, 10 mg of ZnO NPs was used and heated to 1273 K at a heating rate of 10 K min^{-1} under 100 mL min^{-1} of flowing Ar.

A Thermo Scientific Smart iTX accessory with a diamond ATR was used to acquire FTIR spectra of the ZnO nanopowders. The resulting spectra are an average of 50 scans at 4 cm^{-1} resolution using a deuterated triglycine sulfate (DTGS) detector.

2.2.3. DMMP Adsorption/Decomposition on ZnO. A Harrick Scientific Praying Mantis DRA optical accessory was used with an associated Harrick Scientific high temperature reaction chamber HVC-DRP-5 and temperature controller unit (110 V, ATC-024-3) for the diffuse reflectance infrared Fourier transform spectroscopy (DRIFTS) measurements. In a typical experiment, ZnO nanopowder was loosely packed in an environmental DRIFTS cell and heated to 773 K in O_2 for 1 h to remove adsorbed water and carbonates from the ZnO nanoparticles. The ZnO nanoparticles were then cooled to room temperature in flowing O_2. The DMMP exposure was performed using a saturator cell kept at 286 K with argon as the carrier gas.[47,48] A total flow rate of 30 mL min^{-1} was used with an estimated DMMP concentration of 75 ppm. A second test was performed by exposing both ZnO nanopowders to DMMP without any heat pretreatment to compare the differences in how DMMP adsorbs depending on the amount of water and carbonates initially adsorbed on the ZnO particles. The same flow rate and concentration of DMMP were used for both tests. A schematic of the DMMP delivery system can be found in the SI (Figure S5). All DRIFTS spectra were collected at 4 cm^{-1} resolution, with Happ-Genzel apodization,[49] Mertz phase correction,[50] and atmospheric suppression on a Nicolet iS-50R spectrometer equipped with a liquid N_2 cooled mercury cadmium telluride (MCT-A) detector. Spectra were averaged every 15 s (25 scans) using the ZnO nanoparticles as the reference spectrum unless noted.

Headspace analysis was performed using transmission FTIR spectroscopy to determine if volatile decomposition products formed when DMMP was exposed to ZnO NPs. A total of 100 mg of ZnO NPs was placed in a Harrick Scientific 10 cm gas cell (49.09 cm^3 volume) under a N_2 atmosphere. After sealing the cell, 10 μL of DMMP was injected into the cell through a rubber septum. FTIR spectra were then collected (0.5 cm^{-1} resolution) of the headspace above the powder at 10 min intervals on a Nicolet 6700 spectrometer equipped with an MCT-A detector; spectra were averaged over 64 scans followed by a 9.25 min delay.

3. RESULTS

3.1. Adsorption of DMMP on ZnO and the Effect of Water and Hydroxyls. *3.1.1. Modeling of DMMP Adsorption on a Pristine and Hydroxylated ZnO $(10\bar{1}0)$ Surface.* DMMP typically interacts with one of the under-coordinated surface metal atoms, which are Zn atoms with a reduced coordination number relative to the Zn atoms in the bulk (see SI for more details). Additionally, DMMP can adsorb to water and hydroxyls on metal oxide surfaces through its phosphoryl oxygen. In simulating DMMP adsorption on a pristine and hydroxylated ZnO surface, we modeled several adsorption configurations, which are depicted in Figure 3. To compare the results of our DFT modeling and DRIFTS measurements, we calculated vibrational frequencies of a DMMP molecule adsorbed on a pristine and hydroxylated surface as the latter would be the most field relevant.[41,45] Vibrational frequencies calculated for the most favorable adsorption configurations (i.e., highest adsorption energy) are collected in Table 1 along with experimental data, whereas vibrational frequencies calculated for all other configurations are shown in the Supporting Information Table S1.

For DMMP adsorbed on a pristine ZnO surface, our modeling revealed several adsorption configurations (Figure 3a) with relatively close adsorption energies (125−142 kJ mol^{-1}). Configuration **1** (Figure 3a) has the highest adsorption energy (−142.0 kJ mol^{-1}) on a pristine surface. For all adsorption configurations of DMMP on a pristine surface, large red shifts were predicted for the ν(P═O) (~70−90 cm^{-1}) and ν(C−O) (9−30 cm^{-1}) modes relative to the isolated molecule

DOI: 10.1021/acscatal.8b02999
ACS Catal. 2019, 9, 902−911

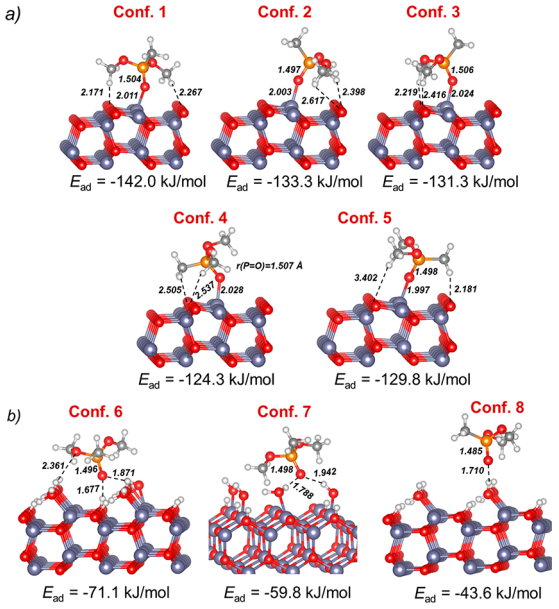

Figure 3. Adsorption configurations of DMMP (a) on a pristine and (b) on a hydroxylated ZnO ($10\bar{1}0$) surface.

(i.e., gas phase DMMP). These calculated shifts are in good agreement with Bermudez's computational studies of DMMP adsorption on γ-Al_2O_3 where he calculated shifts in the ν(P═O) and ν(C−O) modes of −84 and −32 cm^{-1}, respectively.[51,52] Our calculations of the DMMP bond distances for the isolated and adsorbed molecule on the ZnO surface revealed an elongation of the P═O and C−O bonds, which explains the red shift in the ν(P═O) and ν(C−O) modes (see Table S1 of SI).

Several possible adsorption configurations of DMMP on a ZnO surface covered with a water monolayer and their corresponding adsorption energies are depicted in Figure 3b. Configuration **6**, where DMMP interacts with the surface hydroxyls through its phosphoryl and methoxy oxygen atoms, is the energetically most favorable configuration on a hydroxylated ZnO surface and corresponds to the highest adsorption energy (−71.1 kJ mol^{-1}). In configuration **6**, the ν(P═O) mode is red-shifted by 51 cm^{-1}, whereas the ν(C−O) modes are only shifted by 5−10 cm^{-1} relative to the gas phase. In configuration **7**, which is less probable than configuration **6**, DMMP interacts with surface water and hydroxyl groups only through its phosphoryl oxygen. In this configuration, the ν(P═O) and ν(C−O) modes are red-shifted relative to gas phase by 72 cm^{-1} and 9−12 cm^{-1}, respectively (see Table 1).

3.1.2. Water Desorption and Adsorption Analysis of ZnO Nanoparticles. We began our experimental study with the water adsorption properties of ZnO, as the calculations showed that the water and hydroxylation state of ZnO drastically change the energetics of DMMP adsorption and the position of the ν(P═O) and ν(C−O) modes. TGA-MS of both as received ZnO NPs (Figure 4) indicate they have adsorbed

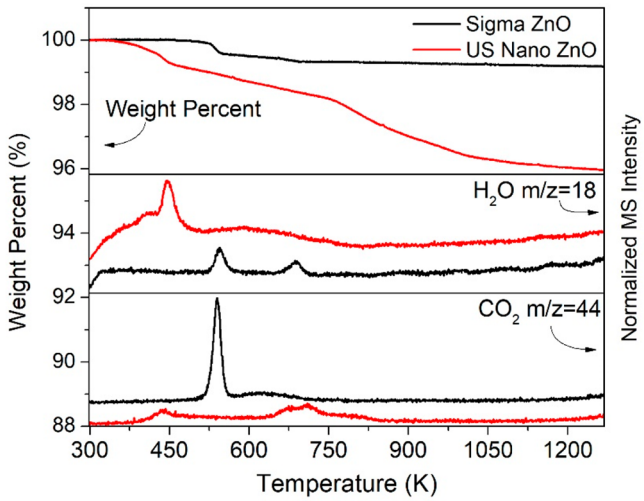

Figure 4. TGA-MS of ZnO nanoparticles heated to 1273 at 10 K min^{-1}.

water and surface carbonate species based on the m/z 18 and m/z 44 ion intensities, respectively, that were measured during heating (393−803 K), which is consistent with the detected weight losses from TGA. The gas phase CO_2 detected is from adsorbed carbonate species that have been described in more detail on a variety of metal oxides including MgO, ZrO_2, and ZnO.[14,53,54] The differences in the weight loss percentages and water/CO_2 release temperatures of the two different ZnO nanopowders can be explained by the differences in the particle

Table 1. Vibrational Frequencies (cm^{-1}) of DMMP in the Gas Phase and Adsorbed on a ZnO Surface, Shifts with Respect to Gas Phase DMMP in Parentheses

		ν(P═O)	ν(C−O) (a)	ν(C−O) (s)
experiment (heated ZnO)[a]	gas	1276	1076	1050
	US Nano ZnO	1220 (−56)	1068 (−8)	1046 (−4)
	Sigma ZnO	1227 (−49)	1065 (−11)	1041 (−9)
experiment (untreated ZnO)[a]	US Nano ZnO	1222 (−54)	1067 (−9)	1050 (0)
	Sigma ZnO	1235 (−41)	1063 (−13)	1039 (−11)
DFT	gas	1205	1090	1054
	ZnO pristine surface			
	conf. **1**	1113 (−92)	1060 (−30)	1033 (−21)
	conf. **2**	1138 (−67)	1077 (−13)	1045 (−9)
	ZnO surface with water monolayer			
	conf. **6**	1154 (−51)	1080 (−10)	1059 (+5)
	conf. **7**	1132 (−72)	1078 (−12)	1045 (−9)

[a]Note: Vibrational frequencies experimentally determined were from DRIFTS spectra of DMMP adsorbed within first 5 min of exposure. With longer exposure, vibrational frequencies begin to align more closely with liquid DMMP from multilayer DMMP adsorption on nanoparticles.

DOI: 10.1021/acscatal.8b02999
ACS Catal. 2019, 9, 902−911

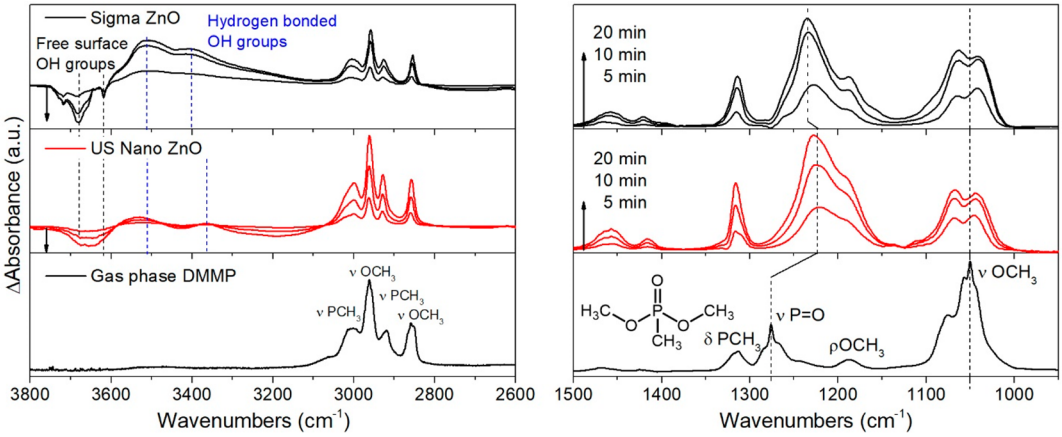

Figure 5. DRIFTS spectra of DMMP adsorbed on heat treated Sigma ZnO (top) and US Nano ZnO (middle) NPs compared to gas phase DMMP spectrum (bottom). DRIFTS spectra of DMMP adsorbed on ZnO are shown after 5, 10, and 20 min of exposure. Arrows indicate increasing or decreasing peak intensity with longer exposure time.

sizes and surface areas of the two commercial powders. A rough estimate of the weight loss for the two nanoparticle samples assuming monolayer coverage of H_2O yields 3.3 and 1.0% for US Nano and Sigma ZnO, respectively, and is close to what is observed in the TGA (~4.0 and 0.8%, respectively). This implies that the surface of ZnO is terminated with mainly hydroxyls and adsorbed water even though ATR-FTIR spectra of the NPs (Figure S4) and mass spectrometry also confirmed the presence of adsorbed carbonates. High temperature DRIFTS analysis also revealed that both types of ZnO nanoparticles begin to hydroxylate upon cooling from 773 K to room temperature (SI Figure S6). This rapid hydroxylation of ZnO is not uncommon and has been observed on other metal oxides. Newberg et al. has performed an ambient pressure X-ray photoelectron spectroscopic (AP-XPS) analysis of a ZnO (10$\bar{1}$0) surface in the presence of water vapor and observed an onset of hydroxylation at 1×10^{-4} % RH.[55] This is 2 orders of magnitude lower than what was observed for other metal oxides, such as Fe_3O_4 and MgO.[56−58] In light of our results, we believe that hydroxylated ZnO is a more realistic model when considering the interactions between nerve agents and ZnO materials that will be used in various ambient environments.

3.1.3. DRIFTS of DMMP Adsorbed on ZnO Nanoparticles. DMMP interactions with activated ZnO NPs (preheated to 773 K for 1 h) were evaluated after 20 min of exposure. The DRIFTS spectra are shown in Figure 5 and compared with our measured transmission FTIR spectrum of gas phase DMMP, which aligns well with the literature.[9,59] For both ZnO nanoparticles, DMMP strongly adsorbs through the P═O, which is shown by the large redshift of the P═O vibration with respect to gas phase DMMP. The O−CH_3 stretching vibration and the other observable vibrational modes of DMMP show no significant shift with respect to gas phase DMMP, which suggests that DMMP has only weak interactions with the ZnO surface through its methoxy moiety. The experimentally observed small red shifts in the C−O stretching (Table 1: 0−13 cm^{-1}) and large shifts in the P═O (41−56 cm^{-1}) of adsorbed DMMP on ZnO are in good agreement with our DFT vibrational frequency shifts of DMMP on the hydroxylated ZnO surface, shown in Table 1. The calculated frequency shifts indicate smaller red shifts in both the P═O and C−O when DMMP adsorbs to ZnO with a water monolayer as compared to a pristine ZnO surface. DRIFTS also shows that the vibrational frequencies of adsorbed DMMP are not strongly affected by preheating (Table 1 and Figure S7), implying that water/hydroxyls should always play an important role while carbonates have little to no influence on the adsorption and decomposition of organophosphonates under ambient conditions.

The decreasing negative peaks of the "free" surface hydroxyls from 3600 to 3750 cm^{-1} and increasing broad peaks correlated to "bound" surface hydroxyls at ~3400 and 3500 cm^{-1}, with increasing exposure, are also indicative that DMMP is interacting with ZnO surface hydroxyls. Similar spectral features have been observed for DMMP adsorption on silica and alumina surfaces and have been attributed to hydrogen bonding of the P═O and O−CH_3 moieties of DMMP to the OH groups present on silica.[59−61]

The results of DFT computed adsorption energies imply that DMMP should aggressively adsorb to both pristine (~142 kJ mol^{-1}) and hydroxylated (~71 kJ mol^{-1}) ZnO surfaces via its phosphoryl oxygen. Configuration **6** corresponds to the most favorable configuration for DMMP adsorption on a hydroxylated surface where the ν(P═O) mode is red-shifted by 51 cm^{-1} and consistent with results from DRIFTS (41−56 cm^{-1}). Also, the ν(C−O) modes in configuration **6** are shifted by only 5−10 cm^{-1}, which is in good agreement with the results of the DRIFTS measurements (0−13 cm^{-1}). The experimental results obtained by FTIR spectroscopy, TGA-MS, and theoretical modeling all suggest that DMMP is most likely adsorbed on hydroxylated ZnO and that any subsequent decomposition should be considered in this context.

3.2. Decomposition of DMMP on ZnO. *3.2.1. DFT Modeling of DMMP Decomposition on ZnO (10$\bar{1}$0) Surface.* We began our theoretical study of DMMP decomposition on ZnO by modeling reactions on a pristine surface (see Supporting Information). Although these results represent a simplified model and are not relevant to realistic conditions of our DRIFTS and FTIR experiments, this study serves as a useful step before modeling the reactions on a hydroxylated surface. According to our calculations, decomposition of DMMP on a pristine ZnO surface will likely proceed through a cleavage of the P−OCH_3 bond and formation of a surface methoxy group with an overall activation barrier of 170.6 kJ mol^{-1} and reaction energy of −19.7 kJ mol^{-1} (Figure S9).

DOI: 10.1021/acscatal.8b02999
ACS Catal. 2019, 9, 902−911

Methanol elimination is known to be the main channel of DMMP hydrolysis on different metal oxides.[2,12,13] In addition, previous studies find that methanol is typically the only decomposition product of DMMP observed in an appreciable amount at room temperature.[4,5,20] Therefore, in modeling DMMP decomposition on a hydroxylated ZnO surface, we studied only mechanisms involving methanol elimination (Figure 6). We also took into consideration that the standard

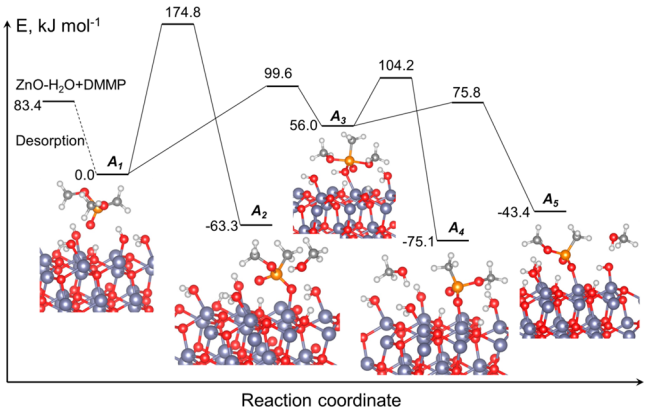

Figure 6. Decomposition of DMMP on ZnO $(10\bar{1}0)$ surface covered with a water monolayer (PBE0-D2-calculated energies are shown relative to the most energetically favorable adsorption configuration of DMMP on a hydroxylated ZnO surface, configuration **6** in Figure 3b).

PBE functional usually tends to underestimate activation barriers of chemical reactions and does not account for vdW interactions.[62−65] Therefore, we refined energies of the reagent, transition state structures, reaction intermediates, and products depicted in Figure 6 using a hybrid PBE0-D2[42,43,66] functional. Results obtained using the PBE functional are collected in the Supporting Information.

The DMMP adsorption energy on hydroxylated ZnO was recalculated using the PBE0-D2 functional and is ∼12 kJ mol^{-1} higher (−83.4 kJ mol^{-1}, Figure 6) than the adsorption energy obtained using the PBE-D2 functional (−71.1 kJ mol^{-1}, Figure 3, Table 1). Elimination of methanol from DMMP adsorbed on the ZnO surface covered with a monolayer of water can proceed via several channels. The first channel ($\mathbf{A_1}$-$\mathbf{A_2}$) is a one step process involving migration of hydrogen from a surface hydroxyl to a methoxy oxygen of DMMP, which breaks the P−OCH_3 bond. The calculated activation barrier and reaction energy of this process are 174.8 kJ mol^{-1} and −63.3 kJ mol^{-1}, respectively. However, there are more energetically favorable reaction pathways $\mathbf{A_1}$-$\mathbf{A_3}$-$\mathbf{A_4}$ and $\mathbf{A_1}$-$\mathbf{A_3}$-$\mathbf{A_5}$ that proceed through the formation of the reaction intermediate $\mathbf{A_3}$ in which a lone pair of electrons from a surface hydroxyl coordinates to the DMMP to give a 5-fold coordinated phosphorus atom. The reaction step $\mathbf{A_1}$-$\mathbf{A_3}$ has an activation barrier of 99.6 kJ mol^{-1}, whereas the intermediate structure $\mathbf{A_3}$ lies 56.0 kJ mol^{-1} higher than $\mathbf{A_1}$.

There are two possible ways to decompose DMMP to form methanol from the intermediate structure $\mathbf{A_3}$. One pathway is shown in the reaction step $\mathbf{A_3}$-$\mathbf{A_4}$, which involves an intramolecular hydrogen transfer and subsequent splitting of the P−OCH_3 bond, which requires 48.2 kJ mol^{-1}. The alternative channel $\mathbf{A_3}$-$\mathbf{A_5}$ proceeds through an intermolecular hydrogen transfer from the surface water molecule and splitting of the corresponding P−OCH_3 bond and only requires 19.8 kJ mol^{-1}. We conclude that decomposition of DMMP on a ZnO surface covered with a monolayer of water will proceed through the channel $\mathbf{A_1}$-$\mathbf{A_3}$-$\mathbf{A_5}$ with an overall activation barrier of 99.6 kJ mol^{-1} and reaction energy of −43.4 kJ mol^{-1}.

3.2.2. Gas Phase Analysis of DMMP Catalysis on ZnO. The DRIFTS analysis and DFT modeling suggest that DMMP will adsorb on the surface hydroxyls of the ZnO nanoparticles mainly through the P═O and only weak interactions through its methoxy moieties. DMMP decomposition on the ZnO NPs has also been confirmed by analyzing the headspace of the gas cell containing ZnO NPs in the presence of DMMP using FTIR spectroscopy shown in Figure 7. Decomposition of

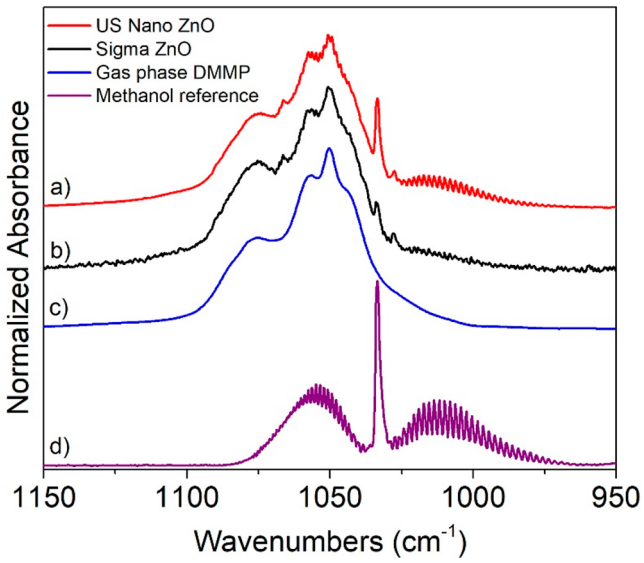

Figure 7. Analysis of headspace by transmission FTIR spectra of (a) US Nano and (b) Sigma ZnO nanoparticles exposed to DMMP, showing methanol formation indicated by a sharp peak at 1033 cm^{-1}. (c) DMMP gas phase spectrum and (d) methanol gas phase spectrum are shown for comparison.

DMMP into methanol readily occurs on both ZnO nanoparticle samples, which is supported by the presence of the peak at 1033 cm^{-1}. The large difference in intensities of the peak at 1033 cm^{-1} is most likely from the differences in the surface areas of the two ZnO nanopowders. Klabunde et al. has found a similar result that nanocrystalline (250−500 m^2 g^{-1}) MgO materials are much more reactive toward organophosphorus compounds compared with their MgO microcrystalline (100−160 m^2 g^{-1}) counterparts, and the DMMP decomposed is directly correlated with the MgO surface area.[67] Our DFT calculations suggest that methanol will form from cleavage of the P−OCH_3 moiety of DMMP and is catalyzed by ZnO surface hydroxyls. Previous studies also suggest that methanol formation can be initiated through P−OCH_3 bond cleavage of DMMP.[2,4,9,68] Although DMMP has many potential byproducts[4−6,10,69] (e.g., methanol, dimethyl ether, formaldehyde, CO_2, formic acid), methanol was the only decomposition byproduct detected in the headspace. These results are in good agreement with previous studies[4,5,20] that find methanol as the primary decomposition product from DMMP on other metal oxides at room temperature. In addition, our calculations find that methanol formation from a ZnO hydroxylated surface (99.6 kJ mol^{-1}) is more energetically favorable than DMMP decomposition on a ZnO pristine

DOI: 10.1021/acscatal.8b02999
ACS Catal. 2019, 9, 902−911

surface (170.6 kJ mol^{-1}), which emphasizes the importance of ZnO surface hydroxyls to decompose DMMP.

4. DISCUSSION

While DFT modeling found that the adsorption energies for DMMP on a pristine ZnO at the under-coordinated Zn atom is ~50−70 kJ mol^{-1} higher than a fully hydroxylated ZnO surface, this finding is not directly relevant for practical applications because ZnO appears to be hydroxylated under ambient conditions. The hydroxylation of ZnO at extremely low relative humidity (≤0.01%) and ultrahigh vacuum has been observed with ZnO and other metal oxides as well.[55−58] The water desorption we observed from TGA-MS (Figure 4) and rapid rehydroxylation of ZnO nanoparticles after heat treatment observed from DRIFTS (SI Figure S6) provide strong evidence that ZnO is hydroxylated under ambient conditions. Furthermore, we have theoretical and experimental data to support DMMP adsorption on a hydroxylated surface, which shows that the magnitude of the vibrational frequency shifts between adsorbed and unbound DMMP are smaller for the ν(P═O) and ν(C−O) stretches compared with DMMP adsorbed on pristine ZnO (Table 1, configurations **1** and **6**). DRIFTS analysis also reveals signature peaks that correspond to hydrogen bonded DMMP to surface hydroxyls (Figure 5).[59,60] As our results point to ZnO being in a hydroxylated state under ambient conditions, we will forego any discussion of the calculations performed for DMMP on pristine ZnO (see Supporting Information).

Our DRIFTS studies show that at ambient conditions, DMMP will adsorb through the P═O···O−H hydrogen bonding interaction to surface hydroxyls, and FTIR gas phase analysis reveals subsequent decomposition to form methanol on ZnO. This is in good agreement with the literature that suggests DMMP initially binds to an under-coordinated Lewis acid site or surface hydroxyl through the P═O bond.[2,5,7,9,20] Many of these studies depict a mechanism where DMMP is bound through its P═O directly to an under-coordinated metal acid site before it undergoes decomposition to form methanol.[2,8,70] However, we have shown from our DFT calculations that DMMP can undergo decomposition on a hydroxylated surface without the P═O moiety initially bonded to an under-coordinated Zn atom (Figure 6 $\mathbf{A_1}$-$\mathbf{A_3}$). In addition, we have also shown that this decomposition mechanism on hydroxylated ZnO is more energetically favorable (~70 kJ mol^{-1}) than DMMP decomposition on a pristine ZnO surface where the P═O moiety of DMMP is directly bound to an under-coordinated Zn atom (see SI Figure S9).

There does not appear to be a universal rule for how DMMP decomposes on oxide surfaces in the presence of water or surface hydroxyls; enhancement or inhibition of DMMP decomposition appears to strongly depend on the oxide and its surface morphology. For instance, Balow et al. found that $Zr(OH)_4$ nanoparticles decompose DMMP and produce twice as much methanol in a 100% RH environment compared to a dry N_2 environment.[14] However, no DMMP decomposition (this includes at high temperatures) is observed with SiO_2 even though the primary mode of DMMP binding occurs through the Si−OH groups on the surface.[10,59,60] Our results show that elimination of methanol proceeds through nucleophilic substitution in which a lone pair of electrons of a surface hydroxyl coordinates to the DMMP to give a 5-fold coordinated phosphorus atom (Figure 6; $\mathbf{A_3}$). Although DMMP decomposition is highly dependent on the metal oxide, the calculated activation barrier of 100 kJ mol^{-1} for this process is close to recently reported activation energies of methanol elimination from DMMP on zirconium hydroxide (108 kJ mol^{-1})[22] and zirconium MOFs (85−93 kJ mol^{-1}).[15] This is possibly because these calculated activation energies also depict transition states with 5-fold coordinated phosphorus atoms.[15,22]

To get a more quantitative perspective, we can estimate the DMMP turnover frequency (TOF) using the calculated activation energy barrier to decompose DMMP into methanol (99.6 kJ mol^{-1}) and the DFT calculated site density (S_0) on a hydroxylated ZnO $(10\bar{1}0)$ surface (2.3×10^{18} sites m^{-2}). Assuming from Figure 6 that the rate dependent step is $\mathbf{A_1}$ to $\mathbf{A_3}$, our DFT studies predict a pre-exponential factor (A_{rxn}) of ~10^{11} s^{-1} from $\mathbf{A_1}$ to the transition state (see SI for more details). Using the activation energy barrier for reaction (99.6 kJ mol^{-1}), the reaction rate constant to form methanol (k_{rxn}) is 3.5×10^{-7} s^{-1} at room temperature. To calculate the reaction rate (R_{rxn}), we assume a first order reaction that is dependent on the coverage of DMMP on ZnO sites. If all hydroxylated ZnO sites are fully covered with DMMP, we should expect a $R_{rxn} \sim 8 \times 10^{11}$ molecules of DMMP s^{-1} m^{-2}. The TOF is obtained by normalizing R_{rxn} to the site density (i.e., TOF = R_{rxn}/S_0) to yield a TOF ~ 3.5×10^{-7} s^{-1}. This TOF is relatively low for metal oxide based heterogeneous catalysts that are typically reported (~10^{-4} to 10^2 s^{-1});[71−73] however, it is important to recognize that our results assume the temperature is 298 K. Furthermore, at these low temperatures, small uncertainties in the predicted activation energy barrier can be significant in the resulting TOF. For example, if the barrier to form methanol were lowered by only 20 kJ mol^{-1}, then the TOF would increase by 4 orders of magnitude (TOF ~ 10^{-3} s^{-1}).

Despite the low TOF, we have verified that we can observe this methanol formation experimentally. On the basis of the 100 mg of US Nano ZnO employed in our experiment (surface area of 65 m^2 g^{-1}), from our kinetics, we calculate a methanol production rate of ~5×10^{12} molecules s^{-1}, assuming DMMP decomposes to form methanol in a 1:1 ratio at room temperature, which is a reasonable assumption based on our proposed mechanism and previous literature.[4,6,70] This should give us a methanol concentration of ~45 ppm in the head space of the experiment during 3 h of DMMP exposure, which is well above our detection limit (~5 ppm). This calculation is in good agreement with our experimental observation, which shows significant methanol production during the first 3 h of DMMP adsorption on ZnO.

We note here that theoretical modeling of DMMP adsorption and decomposition was performed only for a single low energy surface facet $(10\bar{1}0)$ of ZnO, and only one model of surface hydroxylation was considered. Nevertheless, assuming there are no other low energy barrier channels for DMMP decomposition, the low TOF implies that the primary function of ZnO would be as a sorbent rather than as a catalytic material in a practical gas mask situation. In addition, the conclusions obtained on studying DMMP, while providing important insight into adsorbent-oxide chemistry, may not be simply extrapolated to the behavior of sarin and other toxic agents on ZnO, which have to be explicitly explored.

DOI: 10.1021/acscatal.8b02999
ACS Catal. 2019, 9, 902−911

5. CONCLUSIONS

Our combined experimental and theoretical investigations of the adsorptive and catalytic properties of DMMP on ZnO found that ZnO surfaces under ambient conditions will be saturated with a layer of hydroxyls and adsorbed water. FTIR spectroscopic analysis determined that DMMP interacts with ZnO surface hydroxyls and decomposes on ZnO to form methanol with an approximate 100 kJ mol^{-1} barrier. Our theoretical modeling revealed that because of the ZnO surface hydroxylation, DMMP does not bind directly to an under-coordinated Zn atom before decomposing (via cleavage of the $P-OCH_3$ moiety) to form methanol. A theoretical estimate of the DMMP turnover frequency of $\sim 3.5 \times 10^{-7}$ s^{-1} is consistent with the methanol we have observed in the head space of our experiment. Nevertheless, this TOF is relatively low for an application as a CWA decomposition material requiring a realistically important catalytic channel. This study provides insight into the development of improved metal oxide based filtration materials that should ideally decompose CWAs in the presence of surface hydroxyls/adsorbed water and exhibit high TOF under ambient conditions.

■ ASSOCIATED CONTENT

Supporting Information

The Supporting Information is available free of charge on the ACS Publications website at DOI: 10.1021/acscatal.8b02999.

A schematic of DRIFTS experimental setup and ZnO NP characterization including XRD, SEM, ATR-FTIR, and DRIFTS analysis of ZnO nanoparticles; DFT modeling of DMMP adsorbed on ZnO $(10\bar{1}0)$ with one water molecule, calculated DMMP vibrational frequencies, DMMP decomposition mechanisms on ZnO $(10\bar{1}0)$ using PBE functional, calculations of the pre-exponential factor for methanol elimination, description of Zn atom coordination in the bulk and surface, and coordinates of structures from DFT calculations (PDF)

■ AUTHOR INFORMATION

Corresponding Authors

*E-mail: mkukla@nsf.gov.
*E-mail: mrz@umd.edu.

ORCID

Jeffrey Owrutsky: 0000-0003-3216-7270
Tao Wu: 0000-0003-3704-275X
Michael R. Zachariah: 0000-0002-4115-3324

Author Contributions

⊥These authors have contributed equally.

Notes

The authors declare no competing financial interest.

■ ACKNOWLEDGMENTS

We gratefully acknowledge the generous support of the U.S. Department of Defense through the Defense Threat Reduction Agency (HDTRA1-12-1-0005 and HDTRA1-15-1-0005). We also thank Jeffrey Long from the Naval Research Lab for the helpful discussions in this work. S.H. also thanks the GAANN Fellowship program for financial support. R.T. and M.M.K. acknowledge support from NSF XSEDE (Grant DMR-130077) and DOE NERSC (Contract DE-AC02-05CH11231) resources, as well as computational resources at the Maryland Advanced Research Computing Center (MARCC) and University of Maryland supercomputing resources (http://hpcc.umd.edu). We also acknowledge the University of Maryland AIMLab for their microscopy resources and assistance.

■ REFERENCES

(1) Morrison, R. W. *NBC Filter Performance*; ECBC-TR-135, U.S. Army Edgewood Chemical and Biological Center: Aberdeen Proving Ground, MD, 2001.
(2) Mitchell, M. B.; Sheinker, V.; Mintz, E. A. Adsorption and Decomposition of Dimethyl Methylphosphonate on Metal Oxides. *J. Phys. Chem. B* **1997**, *101*, 11192−11203.
(3) Cao, L. X.; Segal, S. R.; Suib, S. L.; Tang, X.; Satyapal, S. Thermocatalytic Oxidation of Dimethyl Methylphosphonate on Supported Metal Oxides. *J. Catal.* **2000**, *194*, 61−70.
(4) Sheinker, V. N.; Mitchell, M. B. Quantitative Study of the Decomposition of Dimethyl Methylphosphonate (DMMP) on Metal Oxides at Room Temperature and Above. *Chem. Mater.* **2002**, *14*, 1257−1268.
(5) Mitchell, M. B.; Sheinker, V. N.; Cox, W. W.; Gatimu, E. N.; Tesfamichael, A. B. The Room Temperature Decomposition Mechanism of Dimethyl Methylphosphonate (DMMP) on Alumina-Supported Cerium Oxide− Participation of Nano-Sized Cerium Oxide Domains. *J. Phys. Chem. B* **2004**, *108*, 1634−1645.
(6) Chen, D. A.; Ratliff, J. S.; Hu, X. F.; Gordon, W. O.; Senanayake, S. D.; Mullins, D. R. Dimethyl Methylphosphonate Decomposition on Fully Oxidized and Partially Reduced Ceria Thin Films. *Surf. Sci.* **2010**, *604*, 574−587.
(7) Gordon, W. O.; Tissue, B. M.; Morris, J. R. Adsorption and Decomposition of Dimethyl Methylphosphonate on Y_2O_3 Nanoparticles. *J. Phys. Chem. C* **2007**, *111*, 3233−3240.
(8) Panayotov, D. A.; Morris, J. R. Thermal Decomposition of a Chemical Warfare Agent Simulant (DMMP) on TiO_2: Adsorbate Reactions with Lattice Oxygen as Studied by Infrared Spectroscopy. *J. Phys. Chem. C* **2009**, *113*, 15684−15691.
(9) Rusu, C. N.; Yates, J. T. Adsorption and Decomposition of Dimethyl Methylphosphonate on TiO_2. *J. Phys. Chem. B* **2000**, *104*, 12292−12298.
(10) Henderson, M.; Jin, T.; White, J. A TPD/AES Study of the Interaction of Dimethyl Methylphosphonate with Iron Oxide (.Alpha.-Fe_2O_3) and Silicon Dioxide. *J. Phys. Chem.* **1986**, *90*, 4607−4611.
(11) Ma, S.; Zhou, J.; Kang, Y.; Reddic, J.; Chen, D. Dimethyl Methylphosphonate Decomposition on Cu Surfaces: Supported Cu Nanoclusters and Films on TiO_2 (110). *Langmuir* **2004**, *20*, 9686−9694.
(12) Head, A. R.; Tsyshevsky, R.; Trotochaud, L.; Yu, Y.; Kyhl, L.; Karslıoğlu, O.; Kuklja, M. M.; Bluhm, H. Adsorption of Dimethyl Methylphosphonate on MoO_3: The Role of Oxygen Vacancies. *J. Phys. Chem. C* **2016**, *120*, 29077−29088.
(13) Tang, X.; Hicks, Z.; Wang, L.; Ganteför, G.; Bowen, K. H.; Tsyshevsky, R.; Sun, J.; Kuklja, M. M. Adsorption and Decomposition of Dimethyl Methylphosphonate on Size-Selected $(MoO_3)_3$ Clusters. *Phys. Chem. Chem. Phys.* **2018**, *20*, 4840−4850.
(14) Balow, R. B.; Lundin, J. G.; Daniels, G. C.; Gordon, W. O.; McEntee, M.; Peterson, G. W.; Wynne, J. H.; Pehrsson, P. E. Environmental Effects on Zirconium Hydroxide Nanoparticles and Chemical Warfare Agent Decomposition: Implications of Atmospheric Water and Carbon Dioxide. *ACS Appl. Mater. Interfaces* **2017**, *9*, 39747−39757.
(15) Wang, G.; Sharp, C.; Plonka, A. M.; Wang, Q.; Frenkel, A.; Guo, W.; Hill, C.; Smith, C.; Kollar, J.; Troya, D.; Morris, J. R. Mechanism and Kinetics for Reaction of the Chemical Warfare Agent Simulant, DMMP (g), with Zirconium (IV) MOFs: An Ultrahigh-Vacuum and DFT Study. *J. Phys. Chem. C* **2017**, *121*, 11261−11272.
(16) Head, A. R.; Tsyshevsky, R.; Trotochaud, L.; Yu, Y.; Karslıoğlu, O.; Eichhorn, B.; Kuklja, M. M.; Bluhm, H. Dimethyl Methyl-

DOI: 10.1021/acscatal.8b02999
ACS Catal. 2019, 9, 902−911

phosphonate Adsorption and Decomposition on MoO_2 as Studied by Ambient Pressure X-Ray Photoelectron Spectroscopy and DFT Calculations. *J. Phys.: Condens. Matter* **2018**, *30*, 134005−134013.
(17) Trotochaud, L.; Tsyshevsky, R.; Holdren, S.; Fears, K.; Head, A. R.; Yu, Y.; Karslıoğlu, O.; Pletincx, S.; Eichhorn, B.; Owrutsky, J.; Long, J.; Zachariah, M.; Kuklja, M. M.; Bluhm, H. Spectroscopic and Computational Investigation of Room-Temperature Decomposition of a Chemical Warfare Agent Simulant on Polycrystalline Cupric Oxide. *Chem. Mater.* **2017**, *29*, 7483−7496.
(18) Kim, K.; Tsay, O. G.; Atwood, D. A.; Churchill, D. G. Destruction and Detection of Chemical Warfare Agents. *Chem. Rev.* **2011**, *111*, 5345−5403.
(19) Jang, Y. J.; Kim, K.; Tsay, O. G.; Atwood, D. A.; Churchill, D. G. Update 1 of: Destruction and Detection of Chemical Warfare Agents. *Chem. Rev.* **2015**, *115*, PR1−PR76.
(20) Panayotov, D. A.; Morris, J. R. Uptake of a Chemical Warfare Agent Simulant (DMMP) on TiO_2: Reactive Adsorption and Active Site Poisoning. *Langmuir* **2009**, *25*, 3652−3658.
(21) Klabunde, K. J.; Park, D. G.; Stark, J. V.; Koper, O.; Decker, S.; Jiang, Y.; Lagadic, I. In *Fine Particles Science and Technology: From Micro to Nanoparticles*; Pelizzetti, E., Ed.; Springer: Dordrecht, The Netherlands, 1996; pp 691−706.
(22) Schweigert, I. V.; Gunlycke, D. Hydrolysis of Dimethyl Methylphosphonate by the Cyclic Tetramer of Zirconium Hydroxide. *J. Phys. Chem. A* **2017**, *121*, 7690−7696.
(23) Martinez-Suarez, L.; Siemer, N.; Frenzel, J.; Marx, D. Reaction Network of Methanol Synthesis over Cu/ZnO Nanocatalysts. *ACS Catal.* **2015**, *5*, 4201−4218.
(24) Gu, X.-K.; Qiao, B.; Huang, C.-Q.; Ding, W.-C.; Sun, K.; Zhan, E.; Zhang, T.; Liu, J.; Li, W.-X. Supported Single Pt_1/Au_1 Atoms for Methanol Steam Reforming. *ACS Catal.* **2014**, *4*, 3886−3890.
(25) Bu, Y.; Weststrate, C.; Niemantsverdriet, J.; Fredriksson, H. O. Role of ZnO and CeO_x in Cu-Based Model Catalysts in Activation of H_2O and CO_2 Dynamics Studied by in Situ Ultraviolet−Visible and X-Ray Photoelectron Spectroscopy. *ACS Catal.* **2016**, *6*, 7994−8003.
(26) Schumann, J.; Eichelbaum, M.; Lunkenbein, T.; Thomas, N.; Alvarez Galvan, M. C.; Schlögl, R.; Behrens, M. Promoting Strong Metal Support Interaction: Doping ZnO for Enhanced Activity of Cu/ZnO: M (M= Al, Ga, Mg) Catalysts. *ACS Catal.* **2015**, *5*, 3260−3270.
(27) Patil, L.; Bari, A.; Shinde, M.; Deo, V.; Kaushik, M. Detection of Dimethyl Methyl Phosphonate−a Simulant of Sarin: The Highly Toxic Chemical Warfare−Using Platinum Activated Nanocrystalline ZnO Thick Films. *Sens. Actuators, B* **2012**, *161*, 372−380.
(28) Pei, Z. F.; Ma, X. F.; Ding, P. F.; Zhang, W. M.; Luo, Z. Y.; Li, G. A. Study of a QCM Dimethyl Methylphosphonate Sensor Based on a ZnO-Modified Nanowire-Structured Manganese Dioxide Film. *Sensors* **2010**, *10*, 8275−8290.
(29) Yang, M.; Kim, H. C.; Hong, S.-H. DMMP Gas Sensing Behavior of ZnO-Coated Single-Wall Carbon Nanotube Network Sensors. *Mater. Lett.* **2012**, *89*, 312−315.
(30) Yoo, R.; Cho, S.; Song, M.-J.; Lee, W. Highly Sensitive Gas Sensor Based on Al-Doped ZnO Nanoparticles for Detection of Dimethyl Methylphosphonate as a Chemical Warfare Agent Simulant. *Sens. Actuators, B* **2015**, *221*, 217−223.
(31) Mahato, T. H.; Prasad, G. K.; Singh, B.; Acharya, J.; Srivastava, A. R.; Vijayaraghavan, R. Nanocrystalline Zinc Oxide for the Decontamination of Sarin. *J. Hazard. Mater.* **2009**, *165*, 928−932.
(32) Houskova, V.; Stengl, V.; Bakardjieva, S.; Murafa, N.; Kalendova, A.; Oplustil, F. Zinc Oxide Prepared by Homogeneous Hydrolysis with Thioacetamide, Its Destruction of Warfare Agents, and Photocatalytic Activity. *J. Phys. Chem. A* **2007**, *111*, 4215−4221.
(33) Kiani, A.; Dastafkan, K. Zinc Oxide Nanocubes as a Destructive Nanoadsorbent for the Neutralization Chemistry of 2-Chloroethyl Phenyl Sulfide: A Sulfur Mustard Simulant. *J. Colloid Interface Sci.* **2016**, *478*, 271−279.
(34) Sadeghi, M.; Yekta, S.; Ghaedi, H. Decontamination of Chemical Warfare Sulfur Mustard Agent Simulant by ZnO Nanoparticles. *Int. Nano Lett.* **2016**, *6*, 161−171.
(35) Perdew, J. P.; Burke, K.; Ernzerhof, M. Generalized Gradient Approximation Made Simple. *Phys. Rev. Lett.* **1996**, *77*, 3865−3868.
(36) Blöchl, P. E. Projector Augmented-Wave Method. *Phys. Rev. B: Condens. Matter Mater. Phys.* **1994**, *50*, 17953−17979.
(37) Kresse, G.; Hafner, J. Ab Initio Molecular Dynamics for Liquid Metals. *Phys. Rev. B: Condens. Matter Mater. Phys.* **1993**, *47*, 558−561.
(38) Kresse, G.; Furthmüller, J. Efficiency of Ab-Initio Total Energy Calculations for Metals and Semiconductors Using a Plane-Wave Basis Set. *Comput. Mater. Sci.* **1996**, *6*, 15−50.
(39) Kresse, G.; Furthmüller, J. Efficient Iterative Schemes for Ab Initio Total-Energy Calculations Using a Plane-Wave Basis Set. *Phys. Rev. B: Condens. Matter Mater. Phys.* **1996**, *54*, 11169−11186.
(40) Sawada, H.; Wang, R.; Sleight, A. W. An Electron Density Residual Study of Zinc Oxide. *J. Solid State Chem.* **1996**, *122*, 148−150.
(41) Wöll, C. The Chemistry and Physics of Zinc Oxide Surfaces. *Prog. Surf. Sci.* **2007**, *82*, 55−120.
(42) Wu, X.; Vargas, M.; Nayak, S.; Lotrich, V.; Scoles, G. Towards Extending the Applicability of Density Functional Theory to Weakly Bound Systems. *J. Chem. Phys.* **2001**, *115*, 8748−8757.
(43) Grimme, S. Semiempirical GGA-Type Density Functional Constructed with a Long-Range Dispersion Correction. *J. Comput. Chem.* **2006**, *27*, 1787−1799.
(44) Henkelman, G.; Uberuaga, B. P.; Jónsson, H. A Climbing Image Nudged Elastic Band Method for Finding Saddle Points and Minimum Energy Paths. *J. Chem. Phys.* **2000**, *113*, 9901−9904.
(45) Meyer, B.; Marx, D.; Dulub, O.; Diebold, U.; Kunat, M.; Langenberg, D.; Wöll, C. Partial Dissociation of Water Leads to Stable Superstructures on the Surface of Zinc Oxide. *Angew. Chem., Int. Ed.* **2004**, *43*, 6641−6645.
(46) Heller, R.; McGannon, J.; Weber, A. Precision Determination of the Lattice Constants of Zinc Oxide. *J. Appl. Phys.* **1950**, *21*, 1283−1284.
(47) Buchanan, J. H.; Buettner, L. C.; Butrow, A. B.; Tevault, D. E. *Vapor Pressure of VX*; ECBC-TR-068, U.S. Army Edgewood Chemical Biological Center: Aberdeen Proving Ground, MD, 1999.
(48) Tevault, D. E.; Buchanan, J. H.; Buettner, L. C. Ambient Volatility of DMMP. *Int. J. Thermophys.* **2006**, *27*, 486−493.
(49) Rabolt, J. F.; Bellar, R. The Nature of Apodization in Fourier Transform Spectroscopy. *Appl. Spectrosc.* **1981**, *35*, 132−135.
(50) Sanderson, R.; Bell, E. Multiplicative Correction of Phase Errors in Fourier Spectroscopy. *Appl. Opt.* **1973**, *12*, 266−270.
(51) Bermudez, V. M. Quantum-Chemical Study of the Adsorption of DMMP and Sarin on γ-Al_2O_3. *J. Phys. Chem. C* **2007**, *111*, 3719−3728.
(52) Bermudez, V. M. Computational Study of Environmental Effects in the Adsorption of DMMP, Sarin, and VX on γ-Al_2O_3: Photolysis and Surface Hydroxylation. *J. Phys. Chem. C* **2009**, *113*, 1917−1930.
(53) Gankanda, A.; Cwiertny, D. M.; Grassian, V. H. Role of Atmospheric CO_2 and H_2O Adsorption on ZnO and CuO Nanoparticle Aging: Formation of New Surface Phases and the Impact on Nanoparticle Dissolution. *J. Phys. Chem. C* **2016**, *120*, 19195−19203.
(54) Tsuji, H.; Okamura-Yoshida, A.; Shishido, T.; Hattori, H. Dynamic Behavior of Carbonate Species on Metal Oxide Surface: Oxygen Scrambling between Adsorbed Carbon Dioxide and Oxide Surface. *Langmuir* **2003**, *19*, 8793−8800.
(55) Newberg, J. T.; Goodwin, C.; Arble, C.; Khalifa, Y.; Boscoboinik, J. A.; Rani, S. ZnO($10\bar{1}0$) Surface Hydroxylation under Ambient Water Vapor. *J. Phys. Chem. B* **2018**, *122*, 472−478.
(56) Kendelewicz, T.; Kaya, S.; Newberg, J.; Bluhm, H.; Mulakaluri, N.; Moritz, W.; Scheffler, M.; Nilsson, A.; Pentcheva, R.; Brown, G., Jr X-Ray Photoemission and Density Functional Theory Study of the Interaction of Water Vapor with the Fe_3O_4(001) Surface at Near-Ambient Conditions. *J. Phys. Chem. C* **2013**, *117*, 2719−2733.
(57) Newberg, J. T.; Starr, D. E.; Yamamoto, S.; Kaya, S.; Kendelewicz, T.; Mysak, E. R.; Porsgaard, S.; Salmeron, M. B.; Brown, G. E., Jr.; Nilsson, A.; Bluhm, H. Formation of Hydroxyl and

DOI: 10.1021/acscatal.8b02999
ACS Catal. 2019, 9, 902−911

Water Layers on MgO Films Studied with Ambient Pressure XPS. *Surf. Sci.* **2011**, *605*, 89−94.
(58) Newberg, J. T.; Starr, D. E.; Yamamoto, S.; Kaya, S.; Kendelewicz, T.; Mysak, E. R.; Porsgaard, S.; Salmeron, M. B.; Brown, G. E., Jr; Nilsson, A.; Bluhm, H. Autocatalytic Surface Hydroxylation of MgO(100) Terrace Sites Observed under Ambient Conditions. *J. Phys. Chem. C* **2011**, *115*, 12864−12872.
(59) Wilmsmeyer, A. R.; Uzarski, J.; Barrie, P. J.; Morris, J. R. Interactions and Binding Energies of Dimethyl Methylphosphonate and Dimethyl Chlorophosphate with Amorphous Silica. *Langmuir* **2012**, *28*, 10962−10967.
(60) Kanan, S. M.; Tripp, C. P. An Infrared Study of Adsorbed Organophosphonates on Silica: A Prefiltering Strategy for the Detection of Nerve Agents on Metal Oxide Sensors. *Langmuir* **2001**, *17*, 2213−2218.
(61) Bermudez, V. M. Effect of Humidity on the Interaction of Dimethyl Methylphosphonate (DMMP) Vapor with SiO_2 and Al_2O_3 Surfaces, Studied Using Infrared Attenuated Total Reflection Spectroscopy. *Langmuir* **2010**, *26*, 18144−18154.
(62) Tsyshevsky, R. V.; Sharia, O.; Kuklja, M. M. Thermal Decomposition Mechanisms of Nitroesters: Ab Initio Modeling of Pentaerythritol Tetranitrate. *J. Phys. Chem. C* **2013**, *117*, 18144−18153.
(63) Kuklja, M. M.; Tsyshevsky, R. V.; Sharia, O. Effect of Polar Surfaces on Decomposition of Molecular Materials. *J. Am. Chem. Soc.* **2014**, *136*, 13289−13302.
(64) Sadhukhan, S.; Muñoz, D.; Adamo, C.; Scuseria, G. E. Predicting Proton Transfer Barriers with Density Functional Methods. *Chem. Phys. Lett.* **1999**, *306*, 83−87.
(65) Nachimuthu, S.; Gao, J.; Truhlar, D. G. A Benchmark Test Suite for Proton Transfer Energies and Its Use to Test Electronic Structure Model Chemistries. *Chem. Phys.* **2012**, *400*, 8−12.
(66) Adamo, C.; Barone, V. Toward Reliable Density Functional Methods without Adjustable Parameters: The PBE0Model. *J. Chem. Phys.* **1999**, *110*, 6158−6170.
(67) Klabunde, K. J.; Stark, J.; Koper, O.; Mohs, C.; Park, D. G.; Decker, S.; Jiang, Y.; Lagadic, I.; Zhang, D. Nanocrystals as Stoichiometric Reagents with Unique Surface Chemistry. *J. Phys. Chem.* **1996**, *100*, 12142−12153.
(68) Trubitsyn, D. A.; Vorontsov, A. V. Experimental Study of Dimethyl Methylphosphonate Decomposition over Anatase TiO_2. *J. Phys. Chem. B* **2005**, *109*, 21884−21892.
(69) Li, Y. X.; Schlup, J. R.; Klabunde, K. J. Fourier Transform Infrared Photoacoustic Spectroscopy Study of the Adsorption of Organophosphorus Compounds on Heat-Treated Magnesium Oxide. *Langmuir* **1991**, *7*, 1394−1399.
(70) Templeton, M. K.; Weinberg, W. H. Adsorption and Decomposition of Dimethyl Methylphosphonate on an Aluminum Oxide Surface. *J. Am. Chem. Soc.* **1985**, *107*, 97−108.
(71) Wachs, I. E.; Routray, K. Catalysis Science of Bulk Mixed Oxides. *ACS Catal.* **2012**, *2*, 1235−1246.
(72) Over, H.; Schomäcker, R. What Makes a Good Catalyst for the Deacon Process? *ACS Catal.* **2013**, *3*, 1034−1046.
(73) Vajda, S.; White, M. G. Catalysis Applications of Size-Selected Cluster Deposition. *ACS Catal.* **2015**, *5*, 7152−7176.

DOI: 10.1021/acscatal.8b02999
ACS Catal. 2019, 9, 902−911